

Classification of the phonon-focusing patterns of tetragonal crystals

A. G. Every

Department of Physics, University of the Witwatersrand, Johannesburg, Wits 2050, South Africa

(Received 4 November 1987)

A classification scheme for the long-wavelength phonon-focusing patterns of nonpiezoelectric tetragonal crystals is proposed. On the basis of their overall appearance and the most prominent features they contain, these patterns can be grouped into 11 categories labeled A, B, C, \dots, K . In most cases the focusing patterns of tetragonal crystals can be traced to the much simpler and more symmetric focusing patterns of transversely isotropic media. In such cases two parameters R_2 and Δ are a good indicator of the type of focusing pattern. Δ is a measure of the deviation of the elastic constants from transverse isotropy, and R_2 is a measure of their polar anisotropy. Category- K crystals approximate the condition where the acoustic slowness surface takes the form of three intersecting ellipsoids.

I. INTRODUCTION

Crystals exhibit a rich variety of phonon-focusing patterns,¹ and the classification of these patterns presents an interesting and worthwhile challenge. Knowledge of the phonon-focusing patterns of crystals is used in predicting the outcome of phonon imaging experiments, calculating the boundary limited thermal conductivity, interpreting phonon wind effects, and for a variety of other purposes. Even a limited classification scheme is of value in this context in guiding the choice of materials, suggesting suitable crystal orientations for experiments, etc.

In the long-wavelength limit and the absence of piezoelectricity, the focusing pattern of a crystal is governed by the ratios of its elastic constants. The focusing patterns of cubic crystals, which depend only on the two parameters $a = C_{11}/C_{44}$ and $b = C_{12}/C_{44}$, have been worked out in considerable detail by Every and Stoddart,² Hurley and Wolfe,³ and others.⁴ The focusing patterns of hexagonal crystals depend on four elastic constant ratios, but because they exhibit transverse isotropy, they are a simple matter to categorize.^{5,6} The role of piezoelectric stiffening of the elastic constants on phonon focusing has been surveyed by Every and McCurdy,⁷ and the effect of first-order spatial dispersion has been treated by Every.⁸ Focusing patterns for phonons located well into the dispersive regime have been obtained for a number of individual crystals⁹ but no general classification of the focusing patterns of dispersive phonons appears to have been undertaken as yet.

In classifying the phonon focusing patterns of tetragonal crystals, a formidable problem that has to be faced is that these patterns depend on a total of five elastic constant ratios, and there is no fortuitous simplification, such as transverse isotropy, to be exploited. Some progress has been made by Winternheimer and McCurdy¹⁰ and Musgrave,¹¹ who have established conditions for the existence of cuspidal edges in the wave surface (along which the focusing is singular) at symmetry planes. These conditions, however, give little intimation of the great variability and complexity of the full focusing patterns of

tetragonal crystals.

A completely comprehensive classification scheme, itemizing all the topologically distinct phonon focusing patterns compatible with the thermodynamic constraints on the elastic constants of tetragonal crystals, does not appear a viable or even desirable undertaking at the present time. It would require an inordinate amount of space to document the results, and the number of separate categories would greatly exceed the number of tetragonal crystals whose elastic constants are presently known.

The objectives of this paper are somewhat less ambitious than this. In the first place the survey is limited to actual crystals whose elastic constants are listed in the compilations of Hearmon,¹² and to neighboring regions of elastic constant space. We have not explored highly unlikely scenarios such as where both C_{11} and C_{33} are smaller than C_{44} and C_{66} . Secondly, we have sorted these patterns into a limited number of categories on the basis of their general appearance and the most prominent features they contain, or because they are closely related in some sense. However, because of the delicate interplay between five elastic constant ratios and the variability this allows, it has meant that with few exceptions each member of a category has minor features which distinguish it from the others.

The form of the elastic constant matrix for tetragonal crystals is very similar to that of hexagonal crystals, differing only in that the constraint $C_{11} - C_{12} - 2C_{66} = 0$ does not apply. Not surprisingly, therefore, it turns out that the focusing patterns of most tetragonal crystals, in overall appearance at least, can be recognized as "descended" from the much simpler focusing patterns of hexagonal crystals. Moreover, we find that a very good indicator of the focusing patterns of tetragonal crystals are the values of two parameters, R_2 , which is a measure of the polar anisotropy and Δ , which is a measure of the azimuthal anisotropy. For hexagonal crystals the value of R_2 determines the existence or not of a certain class of caustics. In some cases we find the focusing patterns of tetragonal crystals bear a close resemblance to those of

cubic crystals. The point of departure in understanding one category of focusing patterns is the condition $C_{13} + C_{44} = C_{12} + C_{66} = 0$, under which the acoustic slowness surface takes the form of three intersecting ellipsoids.

The groundwork for this paper has been laid in an earlier paper⁶ by the author which will be referred to as I. In particular the focusing patterns of hexagonal crystals and the changes that are brought about when the elastic constants are perturbed, and the concepts of avoided intersection caustics and the external conical refraction caustic are explained in much greater detail there.

The results of this paper will primarily be of interest to investigators concerned with the ballistic transport of long-wavelength phonons and acoustic waves in crystals. These results are, however, also relevant to studies of the focusing of large wave-vector phonons, since it is of interest to trace out the evolution of such focusing patterns with frequency, starting at the long-wavelength limit.

II. PHONON FOCUSING: THEORY

A. Phonon imaging

A phonon image portrays the directional dependence of the ballistic phonon flux emanating from a heated spot in an elastically anisotropic crystal.¹³ The nonuniformity of the phonon flux is due to various causes, the most important being bulk phonon focusing.¹⁴ Phonon focusing is usually interpreted in terms of the shape of the phonon constant frequency or slowness surfaces. Phonon group velocity vectors $\mathbf{V} = \nabla_{\mathbf{k}} \omega(k)$ are everywhere normal to the slowness surface and are consequently bunched together in direction, or focused, to an extent inversely proportional to the Gaussian curvature of this surface. A common occurrence is lines of zero Gaussian curvature, or parabolic lines, where the curvature of the slowness surface changes sign. These lines map onto caustics in the phonon intensity, which are a prominent feature of many phonon images.^{3,9,13,15,16}

In the long-wavelength limit, acoustic phonons are governed by the Christoffel equations. Their characteristic equation, which defines the slowness surface,¹⁷⁻¹⁹ is

$$|\Gamma_{rs} - \rho \delta_{rs}| = 0, \quad (1)$$

where Γ_{rs} are the Christoffel coefficients, ρ is the density of the medium and δ_{rs} is the δ function. In the absence of piezoelectricity and dispersion

$$\Gamma_{rs} = C_{rism} S_i S_m, \quad (2)$$

where $\mathbf{S} = \mathbf{k}/\omega$ is the acoustic slowness vector, and C_{rism} is the elastic constant tensor of the medium. For tetragonal crystals lacking a center of inversion the C_{rism} should be replaced by piezoelectrically stiffened elastic moduli. Tetragonal crystals for which the electromechanical coupling is strong enough to significantly influence their phonon focusing, notably BaTiO_3 and related compounds, are relatively few in number, and the results of stiffening have in any case been described by Every and McCurdy.⁷ In the present paper we therefore do not take any ac-

count of piezoelectric stiffening. The effects of first order spatial dispersion, which are most strongly felt in the phonon focusing near to acoustic axes, have been treated by Every,⁸ and will not be pursued in this paper either.

Crystals belonging to the Laue tetragonal group *TI* (crystal classes 422 , $4mm$, $42m$, and $4/mmm$) have six independent elastic constants.²⁰ In the contracted Voigt notation these are $C_{11} = C_{22}$, C_{33} , $C_{44} = C_{55}$, C_{66} , C_{12} , and $C_{13} = C_{23}$. Laue group *III* crystals (classes 4 , $\bar{4}$, and $4/m$) possess an additional independent elastic constant C_{16} .

We have used the standard Monte Carlo method of constructing theoretical phonon images^{13,6} which consists in generating a uniform random distribution of phonon wave normals \mathbf{n} , calculating their associated ray vectors \mathbf{V} , and sorting these in direction to form a polar plot of the phonon intensity. The intensity plots presented in this paper have each been generated from approximately 3×10^5 symmetry inequivalent \mathbf{n} 's, and the \mathbf{V} 's have been stored in a 512×512 array. The printing has been done with a laser printer, outputting the value of each array element as a matrix of 3×3 dots either on or off. The darkness of the plots denotes phonon intensity.

B. Phonon focusing near to acoustic axes

The occurrence of acoustic axes, i.e., directions in which two or more isonormal acoustic modes are degenerate, has an important bearing on the phonon focusing pattern of a medium.⁶ Two types of degeneracy are generic to tetragonal crystals.²¹ There is always tangential contact between the slow transverse (ST) and fast transverse (FT) sheets of the slowness surface (S) in the $[001]$ direction. In many but not all tetragonal crystals there are points of conical degeneracy between the transverse sheets of S . These are confined to the $\{100\}$, $\{110\}$, and $\{001\}$ planes.

By way of example, Fig. 1(a) shows the ST sheet of S for the crystal $\text{Ag}_2\text{SO}_4 \cdot 4\text{NH}_3$. Elastic constants for all real materials reported on in this paper have been taken from the compilations of Hearmon.¹² There are two classes of conical points, labeled C and C' , which are located in the $\{001\}$ and in the $\{110\}$ planes, respectively. GeO_2 is in an example of a material having conical points in the $\{001\}$ plane only, and terbium molybdate a material having no conical points at all.

At a conical point the polarization field of the degenerate modes possesses a singularity²² of rotary index $n = \pm \frac{1}{2}$ (i.e., in a small excursion around the conical point the polarization field rotates by $2\pi n$ where $n = \pm \frac{1}{2}$). In Fig. 1(a) $n = +\frac{1}{2}$ for C and $n = -\frac{1}{2}$ for C' . In the vicinity of a conical point at least one of the principal curvatures of the ST sheet of S must be negative, while there are necessarily regions elsewhere where both the principal curvatures of this sheet are positive. This implies the existence of parabolic lines and associated caustics in the phonon intensity. As expected, caustics are a prominent feature of the focusing pattern of $\text{Ag}_2\text{SO}_4 \cdot 4\text{NH}_3$ shown in Fig. 1(b). Vesuvian is an example of a tetragonal crystal possessing no conical points and displaying no phonon caustics. The absence of conical points is not, however, a

sufficient condition for the absence of caustics.

At the [001] point of tangential degeneracy the polarization field of the transverse modes has a singularity of rotary index $n = \pm 1$. In the case of $\text{Ag}_2\text{SO}_4 \cdot 4\text{NH}_3$, $n = 1$ as is evident from Fig. 1(a). For some materials, examples of which are provided later in this paper, $n = -1$. For one of the transverse branches the polarization alter-

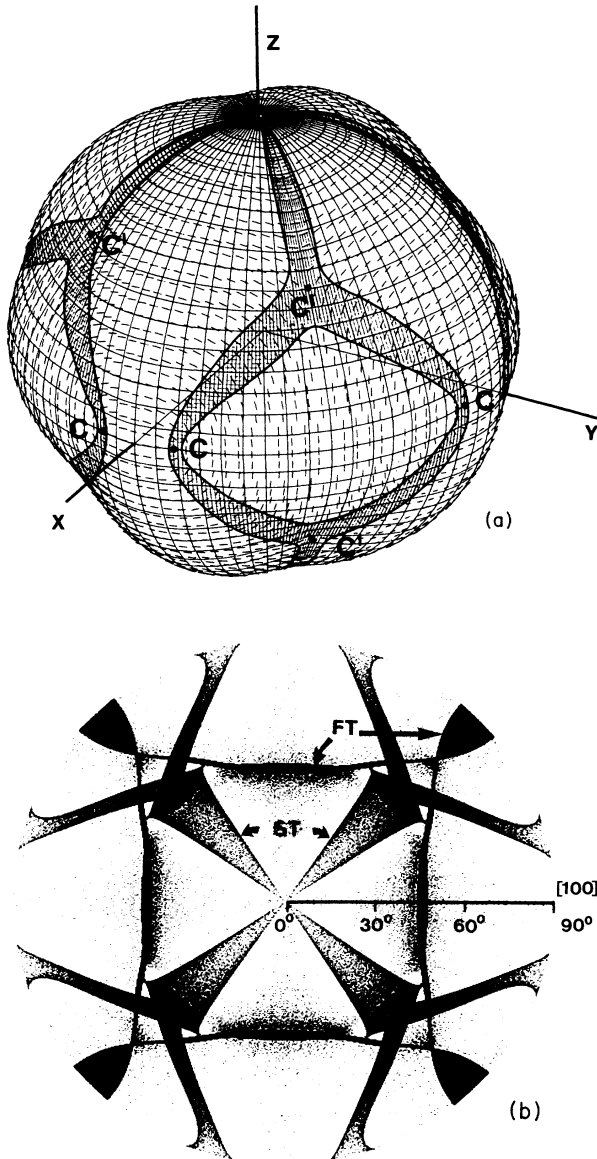


FIG. 1. (a) ST sheet of the acoustic slowness surface of $\text{Ag}_2\text{SO}_4 \cdot 4\text{NH}_3$. The shaded areas represent regions of negative Gaussian curvature, the remainder of the surface being of positive curvature. The polarization field displays singularities at two sets of conical points labeled C and C' . The surface is negatively curved in the region of these conical points. (b) Polar plot of the ST and FT phonon intensity for $\text{Ag}_2\text{SO}_4 \cdot 4\text{NH}_3$. Darkness of the greyscale represents the phonon intensity. Caustics are labeled according to branch. The ST caustics are mapped from the lines of zero Gaussian curvature separating the negatively and positively curved portions of the surface in (a).

nates between pure transverse (PT) normal to the {100} planes and quasitransverse (QT) in the {110} planes. For the other transverse branch the converse applies.

A tangential degeneracy, unlike a conical point, does not in itself imply the existence of caustics. However when there is a strong coupling between the two transverse sheets, and this is particularly true for the case where $n = -1$, one or both of these sheets becomes sufficiently rippled around the [001] direction so that the principal curvatures transverse to the {100} and {110} planes are opposite in sign. There are now alternating wedge-shaped regions of negative and positive Gaussian curvature spreading out from the [001] direction. The parabolic lines separating these regions map onto a set of four line caustics intersecting at the [001] axis. This structure can be seen in the center of the phonon intensity plot for $\text{Ag}_2\text{SO}_4 \cdot 4\text{NH}_3$ in Fig. 1(b).

For special values of the elastic constants higher-order degeneracies can occur. The condition $C_{11} - C_{12} - 2C_{66} = 0$ leads to transverse isotropy, and allows the occurrence of circular lines of wedge-shaped degeneracy around the Z axis where the QT and PT sheets of S intersect.⁶ For $C_{13} + C_{44} = C_{12} + C_{66} = 0$ all the off-diagonal elements of Γ_{rs} vanish and the equation for the slowness surface factorizes, yielding three intersecting ellipsoids. The slightest deviation from the conditions required for line degeneracy lead to the lifting of this degeneracy at all except a finite set of points. The ST sheet now has narrow saddle-shaped strips located near the original intersections. The boundaries of these negatively curved strips map onto a set of caustics which develop globally and grow in intensity as the deviation from the special condition increases. Several examples of such avoided intersection caustics are provided later in this paper.

Special values of the elastic constants can also lead to other "accidental" degeneracies such as triple degeneracies,⁶ but such cases will not be considered here.

III. CHARACTERIZATION OF THE ANISOTROPY OF TETRAGONAL CRYSTALS

The form of the elastic constant matrix of Laue tetragonal group Tl crystals differs from that of hexagonal crystals in only one respect, namely, that the elastic constant combination $C_{11} - C_{12} - 2C_{66}$ is nonzero. It is useful therefore to compare tetragonal crystals to the elastically most similar transversely isotropic hexagonal crystals. A convenient measure of the deviation from transverse isotropy is given by the value of the quantity

$$\Delta = (C_{11} - C_{12} - 2C_{66}) / C_{66}, \quad (3)$$

which we will call the azimuthal anisotropy parameter. For $\Delta = 0$ the focusing pattern has full rotational symmetry about the Z axis. As Δ departs from zero the existing caustics gradually deform, and avoided intersection caustics may materialize. The focusing pattern now has full tetragonal symmetry. Even for fairly large Δ the new focusing pattern often maintains a clear familial resemblance to the original pattern.

The focusing patterns of transversely isotropic media

have been categorized by McCurdy⁵ and in I. For $\Delta=0$ the Christoffel characteristic equation factorizes. One sheet of S is associated with PT modes, and is ellipsoidal in shape. As such it is entirely convex and hence does not give rise to any caustics. The inner quasilongitudinal

sheet is also entirely convex and does not give rise to caustics either. It is only the QT sheet that can have negatively curved regions and yield caustics.

New QT focusing singularities in transversely isotropic media emerge at specific values of the quantities^{6,5}

$$R_1 = (C_{13} + C_{44})^2 / [C_{33}(C_{11} - C_{44})], \quad (4)$$

$$R_2 = \frac{4(C_{13} + C_{11})(C_{13} + C_{33})[(C_{11} - C_{44})(C_{33} - C_{44}) - (C_{13} + C_{44})^2]}{[(C_{13} + C_{11}) + (C_{13} + C_{33})](C_{13} + C_{44})(C_{11}C_{33} - C_{13})^2}, \quad (5)$$

and

$$R_4 = (C_{13} + C_{44})^2 / [C_{11}(C_{33} - C_{44})]. \quad (6)$$

For $R_1 > 1$ the QT sheet is curved inwards near the (001) plane to form a saddle-shaped "waist" as depicted by curve Q1 in Fig. 1 of I. The boundaries of this region map onto circular caustics above and below the (001) plane. For $R_4 > 1$ the QT sheet is concave near the [001] axis, again as depicted by curve Q1 in Fig. 1 of I, and there is a surrounding saddle-shaped region and finally a convex region. The boundary between the saddle-shaped and convex regions maps onto the external conical refraction caustic, which is an intense point caustic along the [001] axis. The boundary between the concave and saddle-shaped regions maps onto a circular caustic. For $R_2 > 1$ the QT sheet has a saddle-shaped region inbetween the [001] axis and the (001) plane, as depicted by curve Q3 in Fig. 1 of I, which brings about pairs of circular caustics above and below the (001) plane.

Although R_1 , R_2 , and R_4 are nominally independent of each other, if the condition $R_2 > 1$ is satisfied then $R_1 > 1$ and $R_4 > 1$ cannot be satisfied and vice versa. Also the values of R_1 and R_4 tend to be very similar. Fig. 2 shows the good correlation that exists between R_1

and R_2 when these are evaluated using the elastic constants of tetragonal crystals listed in the compilations of Hearmon.¹² There is a similarly good correlation between R_4 and R_2 . So, as a rough guide, any one of the three quantities R_1 , R_2 , or R_4 can be used for characterizing the polar anisotropy of a transversely isotropic or nearby tetragonal medium. We have chosen R_2 for this purpose and will refer to it as the polar anisotropy parameter.

A. Range of elastic constants

The elastic constants of TI group crystals are subject to the thermodynamic constraints $C_{11} > 0$, $C_{33} > 0$, $C_{44} > 0$, $C_{66} > 0$, $|C_{12}| < C_{11}$, and $C_{12} > 2C_{13}^2/C_{33} - C_{11}$. There are certain regions of elastic constant space, such as $C_{11}, C_{33} < C_{44}, C_{66}$ where no known crystals occur, which we do not cover in this survey.

A 45° rotation of axes about the Z direction does not alter the form of the elastic constant matrix but transforms the elastic constants in such a way that

$$\Delta \rightarrow \Delta' = -2(C_{11} - C_{12} - 2C_{66}) / (C_{11} - C_{12}), \quad (7)$$

which involves a change in sign. With no loss of generality therefore we have restricted the survey to positive Δ . The additional elastic constant C_{16} of TII group crystals is eliminated by a rotation of axes about the Z direction through an angle ϕ given by¹⁷

$$\tan(4\phi) = 4C_{16} / (C_{11} - C_{12} - 2C_{66}). \quad (8)$$

Two inequivalent angles emerge from this condition, and the one has been chosen that yields a positive value of Δ . With suitable choice of axes TI and TII group crystals thus have the same form of elastic constant matrix and acoustic symmetry, and do not have to be treated separately. This simplification breaks down, however, if there is piezoelectric stiffening of the elastic constants⁷ or dispersion.^{8,20}

IV. CLASSIFICATION OF THE FOCUSING PATTERNS

In proposing the following scheme for the classification of the focusing patterns of tetragonal crystals we have taken into account all the tetragonal crystals listed in the elastic constant compilations of Hearmon¹² as well as many hypothetical media in neighboring regions of elastic constant space. Based on their general overall appear-

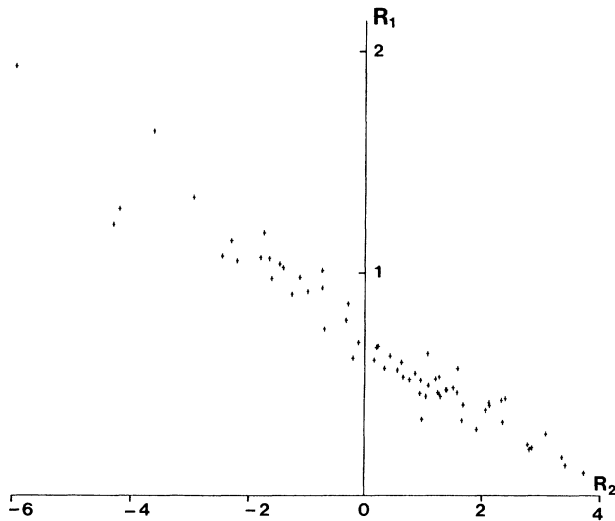


FIG. 2. The distribution of tetragonal crystals on a plot of R_1 vs R_2 , based on elastic constants listed in the compilations of Hearmon (Ref. 12).

TABLE I. Rotation angle ϕ , anisotropy parameters, and phonon-focusing categories for tetragonal crystals, based on data from Ref. 12.

Material	ϕ (deg)	R_1	R_4	R_2	Δ	Category
terbium molybdate	0.000	1.342	1.290	-2.917	0.160	A
SrClF	45.000	0.916	1.038	-0.976	0.082	A
potassium lithium niobate	0.000	0.974	1.788	-1.595	0.086	A
BaClF	45.000	1.070	1.323	-1.783	0.072	A
In-3.42 at. % Cd alloy	45.000	1.076	1.112	-2.431	9.842	B
In	45.000	1.055	1.087	-2.177	7.231	B
In-10 at. % Tl alloy	45.000	1.219	1.262	-4.282	11.935	B
BaTiO ₃	45.000	0.904	1.133	-1.247	2.708	B
AgGaS ₂	45.000	1.146	1.291	-2.279	2.176	B
In-5 at. % Pb alloy	45.000	1.290	1.321	-4.181	4.525	B
InBi	45.000	1.932	3.024	-5.932	2.511	B
CdGeAs ₂	45.000	1.640	2.129	-3.596	2.676	B
CoPt	45.000	1.024	1.217	-1.399	3.073	B
pentaerythritol tetranitrate	0.000	1.066	1.291	-1.630	1.003	B
calcium strontium propionate (261 K)	-9.080	1.040	1.149	-1.455	1.166	B
urea	0.000	1.182	0.953	-1.726	26.444	B?
Zr ₂ Ni	0.000	0.637	0.645	1.067	0.795	C
scapolite	0.000	0.276	0.270	3.075	0.790	C
Al ₂ Cu	0.000	0.416	0.421	2.105	0.406	C
RbH ₂ PO ₄	0.000	0.171	0.180	3.344	17.438	D
RbD ₂ AsO ₄	0.000	0.135	0.144	3.404	14.814	D
RbH ₂ AsO ₄	0.000	0.101	0.110	3.715	14.218	D
KH ₂ AsO ₄	0.000	0.228	0.244	2.765	7.658	D
KH ₂ PO ₄	0.000	0.214	0.227	2.832	10.251	D
KD ₂ PO ₄	0.000	0.206	0.218	2.792	10.323	D
KD ₂ AsO ₄	0.000	0.427	0.432	2.319	8.081	D
NH ₄ H ₂ AsO ₄	0.000	0.383	0.442	2.050	6.617	D
NH ₄ H ₂ PO ₄	0.000	0.407	0.476	1.671	8.349	D
ND ₄ D ₂ PO ₄	0.000	0.337	0.413	1.651	9.000	D
CoF ₂	45.000	0.462	0.465	1.567	9.432	D
SnO ₂	45.000	0.461	0.453	1.236	7.741	D
NiF ₂	45.000	0.474	0.478	1.376	9.360	D
ZnF ₂	45.000	0.524	0.522	1.197	7.782	D
MnF ₂	45.000	0.483	0.481	1.497	11.467	D
LuAsO ₄	0.000	0.453	0.431	1.266	10.938	D
LuPO ₄	0.000	0.443	0.419	1.286	11.088	D
MgF ₂	45.000	0.459	0.466	0.938	5.648	D
CaMoO ₄	64.217	0.445	0.484	1.037	1.926	D
NbO ₂	0.025	0.550	0.569	0.851	4.196	D
K ₂ PtCl ₄	0.000	0.519	0.565	0.946	2.637	D
TiO ₂	45.000	0.522	0.493	0.756	6.348	D
Hg ₂ I ₂	45.000	0.435	0.352	2.383	43.253	E
Hg ₂ Br ₂	45.000	0.404	0.319	2.116	36.621	E
Hg ₂ Cl ₂	45.000	0.329	0.265	2.339	31.600	E
TeO ₂	45.000	0.296	0.309	1.901	64.800	E
Ag ₂ SO ₄ ·4NH ₃	45.000	0.533	0.519	1.259	1.073	F
AgClO ₃	-18.285	0.572	0.594	1.570	0.881	F
CsPbF ₃	45.000	0.932	0.934	-0.729	0.687	G
chrysazin	16.148	0.787	0.570	-0.318	0.517	G
Ba ₂ Si ₂ TiO ₈	45.000	0.343	0.442	0.974	0.269	G
FeGe ₂	0.000	0.495	0.492	1.078	0.486	G
K ₂ CuF ₄	0.000	0.473	0.444	1.391	0.682	G
gadolinium molybdate	0.000	0.533	0.502	0.649	0.296	G
vesuvian	45.000	0.608	0.585	0.158	0.057	G
TlSe	45.000	1.011	0.829	-0.734	0.019	G

TABLE I. (Continued.)

Material	ϕ (deg)	R_1	R_4	R_2	Δ	Category
$\text{Sr}_{0.75}\text{Ba}_{0.25}\text{Nb}_2\text{O}_6$	0.000	0.618	0.803	-0.202	0.258	G
calcium strontium propionate	0.000	0.980	1.046	-1.112	0.513	G
$\text{Sr}_4\text{LiKNb}_{10}\text{O}_{30}$	0.000	0.747	1.037	-0.694	0.000	G
tin	45.000	0.600	0.600	0.625	5.104	H
LiYF_4	-12.818	0.669	0.609	0.222	2.819	H
$\text{LiY}_{0.5}\text{Tb}_{0.5}\text{F}_4$	-14.024	0.627	0.572	0.429	20.781	H?
ZrSiO_4	45.000	0.861	0.835	-0.286	3.728	I
ZnP_2	0.000	0.687	0.732	-0.108	1.673	I
PbMoO_4	61.028	0.664	0.744	0.194	5.046	I
SrMoO_4	57.695	0.572	0.648	0.330	2.826	I
GeO_2	45.000	0.565	0.533	0.550	4.926	I
$\text{NH}_4\text{H}_2\text{PO}_4$ (44% deuterated)	0.000	0.579	0.733	0.479	12.226	J
HgI_2	0.000	0.853	1.197	-1.130	9.861	J
CsH_2AsO_4	0.000	0.036	0.037	8.066	28.024	K
pentaerythritol	13.679	0.320	0.373	2.800	17.032	K
$\text{NiSO}_4 \cdot 6\text{H}_2\text{O}$	45.000	0.190	0.234	1.709	5.911	K
CaWO_4	67.205	0.358	0.386	1.553	2.913	K

ance and the most prominent features that are present in them or because they are closely related in some sense, these focusing patterns can be grouped into 11 main categories *A, B, . . . , K*. Minor distinguishing features that most focusing patterns possess are ignored in making this classification.

Table I lists the real crystals we have taken account of, their values of ϕ , R_1 , R_2 , R_4 , and Δ , and the categories their focusing patterns fall into. Figure 3 shows the approximate location of the various categories on a plot of R_2 versus Δ . Near the boundaries of these domains there can be uncertainty as to the appearance of the focusing pattern, with all the elastic constant ratios independently

exerting their influence. This is particularly true where Δ or R_2 or both are small (< 1) and there is more variability. For Δ and R_2 large the focusing patterns tend to stabilize. There is less variability and the focusing patterns are relatively insensitive to the specific values of the five elastic constant ratios.

The main characteristics of the various categories of focusing patterns are as follows.

Category A: $R_2 < -1, \Delta < 1$

A large negative value of R_2 correlates with $R_1 > 1$ and $R_4 > 1$. In the transverse isotropy limit $\Delta = 0$ there are

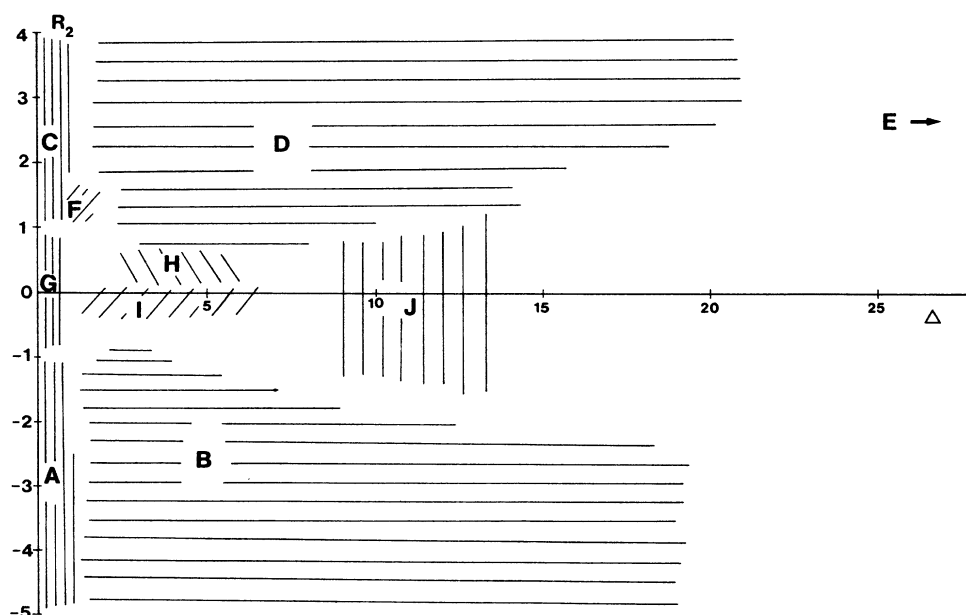


FIG. 3. Approximate location of the various categories of focusing patterns of tetragonal crystals on a plot of R_2 vs Δ .

the external conical refraction caustic, surrounding circular caustic and "waistband" caustic. As can be seen in Fig. 4, which is a phonon intensity plot for Terbium molybdate, the latter two caustics, which are labeled 2 and 1, respectively, are structurally stable against the lowering of the acoustic symmetry by small deviations of Δ from zero. They merely gradually deform from being circular. For 2 this deformation is noticeable in Fig. 4, but for 1 it is barely perceptible.

As Δ deviates from zero the highly degenerate external conical refraction caustic located along the [001] axis transforms into a star-shaped structure comprising eight linked cusps (labeled 3 in Fig. 4). Figure 5(a) displays this structure more clearly. With increasing Δ four of these cusps approach caustic 2, the other four extending beyond 2 and eventually merging with caustic 1. This development is very similar to what occurs when there is a lowering from hexagonal to trigonal symmetry with the deviation of C_{14} from zero, except that in that case there are three cusps of each type instead of four.⁶

Also evident in Fig. 5(a) are a set of precursors labeled 4. These are regions of high but nonsingular focusing that evolve into caustics for larger Δ .

For $C_{44} > C_{66}$ and $\Delta = 0$ the two transverse sheets of S intersect as depicted by curves $Q1$ and $P2$ in Fig. 1 of I, to form lines of wedge-shaped degeneracy. As Δ deviates from zero this degeneracy is lifted everywhere except at a set of eight equidistantly spaced conical points in the $\{100\}$ and $\{110\}$ planes. Four of these have rotary index $n = +\frac{1}{2}$, and the other four have $n = -\frac{1}{2}$. The avoided intersection caustics thus formed, each of which link together eight cusps, are labeled 5 and 5' in Fig. 5(b). A similar development occurs when the symmetry is lowered from hexagonal to trigonal,⁶ but involving six cusps instead of eight.

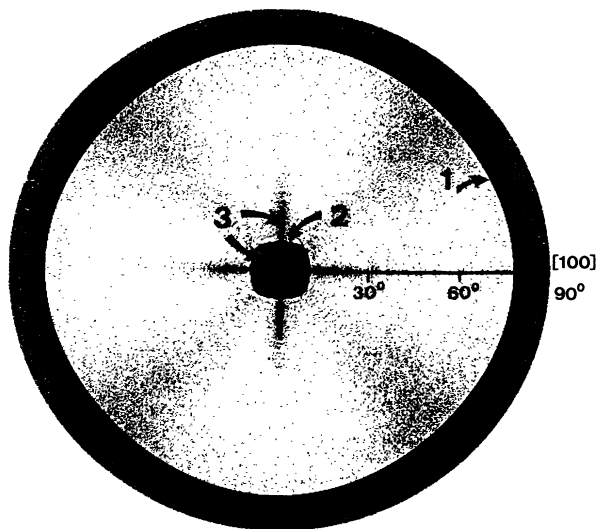


FIG. 4. Polar plot of the ST and FT phonon intensity for terbium molybdate ($\Delta = 0.16$).

Category B: $R_2 < -1, \Delta > 1$

The focusing patterns of representative materials in this category are shown in Fig. 6. Approximately 17% of the tetragonal crystals tabulated by Hearmon¹² fall into this category. The large values of Δ have transformed the precursors 4 into intense caustic structures which are a prominent feature of these focusing patterns.

In the case of InBi [Fig. 6(a)] $|R_2|$ is very large and caustics 1, 2, and 3, even though they have undergone a

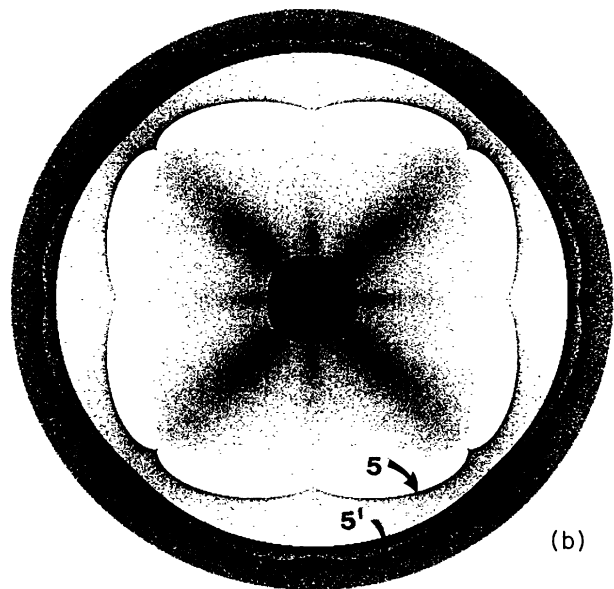
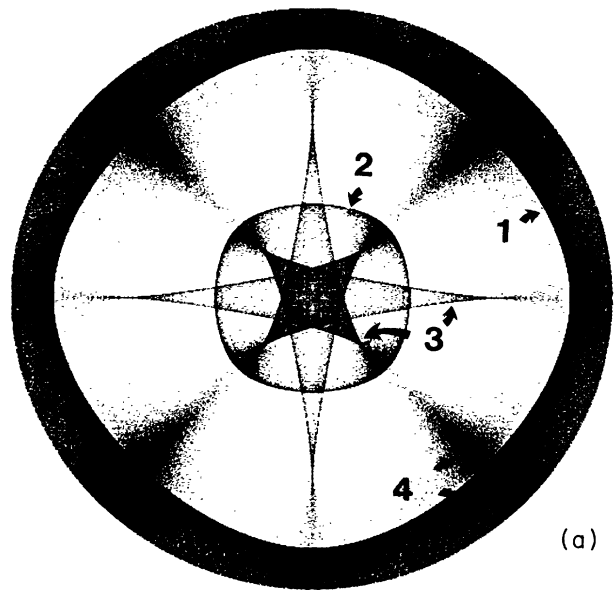


FIG. 5. ST and FT phonon intensity pattern for (a) a hypothetical medium with $C_{11}=4$, $C_{33}=2$, $C_{66}=1.5$, $C_{12}=0.4$, and $C_{13}=2$ and (b) a hypothetical medium with $C_{11}=4$, $C_{33}=4$, $C_{66}=0.7$, $C_{12}=2.5$, and $C_{13}=3$. All elastic constants are in units of C_{44} .

number of changes, are still easily recognizable.

AgGaS₂ [Fig. 6(b)] has a smaller value of $|R_2|$ and the FT caustics 4 are the dominating feature in its focusing pattern. This focusing pattern bears a striking resemblance to that of cubic crystals such as Si and Ge (see Ref. 2). Indeed the elastic constants of AgGaS₂ are within about 10% of satisfying the conditions $C_{11} = C_{33}$, $C_{44} = C_{66}$, and $C_{12} = C_{13}$ required of cubic crystals.

InCd [Fig. 6(c)] is a material with exceptionally large Δ . The FT caustics 4 are very much distended, and the main relic of caustics 1, 2, and 3 is the prevalence of strong focusing near the [001] direction and (001) plane.

Category C: $R_2 > 1, \Delta < 1$

A large positive value of R_2 correlates with $R_1 \ll 1$ and $R_2 \ll 1$. For $\Delta = 0$ the QT sheet of S has a saddle-shaped region lying between the [001] direction and (001) plane. The boundaries of this region map onto circular caustics which are structurally stable against small deviations of Δ from zero. If the QT and PT sheets intersect, when Δ deviates from zero each line of wedge-shaped degeneracy is replaced by a set of eight conical points and avoided intersection caustics 5 and 5' materialize. With increasing Δ precursors 4 appear and eventually evolve

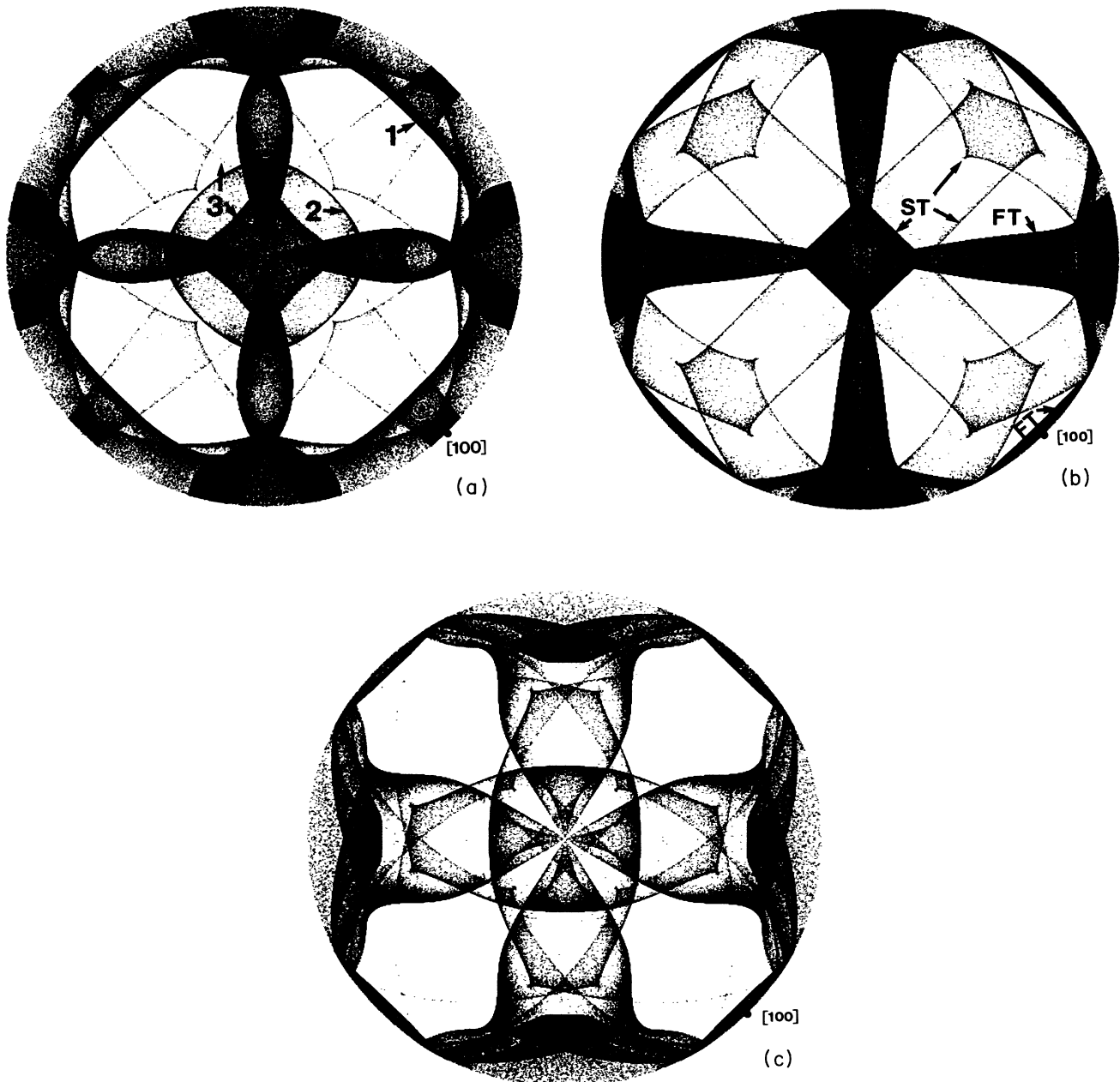


FIG. 6. ST and FT phonon intensity pattern for (a) InBi, (b) AgGaS₂, and (c) In-3.4 at. % Cd alloy.

into caustic structures.

The phonon-focusing pattern of Al_2Cu shown in Fig. 7(a) contains the circular caustics (labeled 6 and 6') as well as the avoided intersection caustics 5 and 5'. The finite value of Δ has caused caustics 5' and 6' to become intertwined. The precursors 4 and 4' are well developed.

Figure 7(b) shows that the focusing pattern of Zr_2Ni is delicately poised near the condition $R_2=1$ at which the caustics 6 and 6' emerge from an intense circular precursor. There are no avoided intersection caustics, but Δ

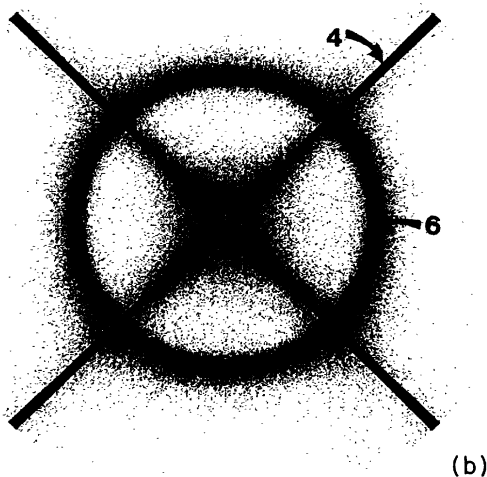
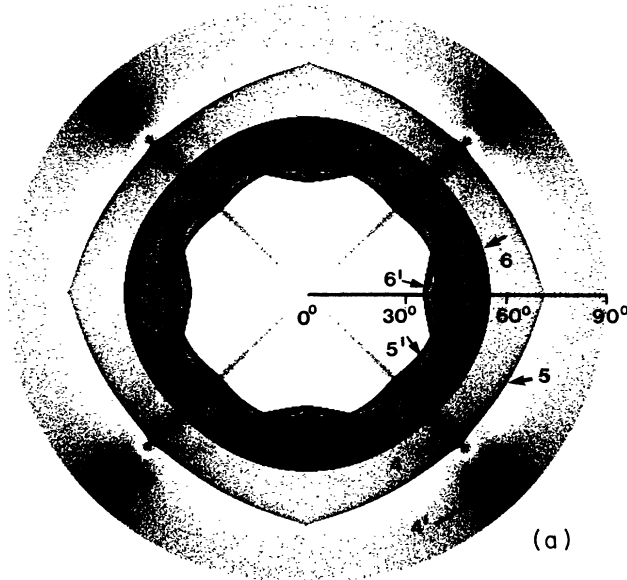


FIG. 7. ST and FT phonon intensity pattern for (a) Al_2Cu , (b) Zr_2Ni ($R_2=1.07$, $\Delta=0.80$).

is large enough that structure 4 has been transformed into caustics.

Category D: $R_2 > 1$, $\Delta > 1$

Approximately 31% of the tetragonal crystals tabulated by Hearmon¹² fall into this category. Representative examples of their focusing patterns are shown in Figs. 8(a), 8(b), and 8(c). With increasing Δ the caustics 6 and 6' deform into a square-shaped structure which becomes entangled with caustics 4, and together these make up the most prominent features in the focusing patterns.

In the case of K_2PtCl_4 [Fig. 8(a)] for which $R_2=0.95$, the square-shaped structure is still partially in the form of precursors. CoF_2 [Fig. 8(b)] has $R_2=1.57$ and the caustics of the square-shaped structure are well separated. RbD_2AsO_4 [Fig. 8(c)] has $R_2=3.40$, which is exceptionally large, and the square-shaped caustics are very far apart. This demonstrates how the excess of R_2 over 1.0 is a good indicator of the separation of the square-shaped caustics.

Figure 8(d) shows the ST sheet of S for K_2PtCl_4 . The negatively curved regions surrounding the conical points C produce the structures labeled ST_1 in Fig. 8(a). This is an example of a material for which the polarization field near the [001] direction has rotary index $n=-1$. The strong interaction between the ST and FT branches near this direction is responsible for the structures labeled ST_2 . The remaining caustics and precursors in Fig. 8(a) belong to the FT branch.

Figure 8(e) shows the FT sheet of S for CoF_2 . The parabolic lines labeled FT_1 and FT_2 map onto similarly labeled caustics in the square-shaped structure of Fig. 8(b).

Category E: $R_2 > 1$, $\Delta \gg 1$

Even for very large values of Δ the square-shaped structure remains intact, but the other structures become highly distended, as the phonon-focusing pattern of Hg_2Br_2 in Fig. 9 shows. The focusing pattern of TeO_2 , which has been studied experimentally by Hurley *et al.*,¹⁶ falls into this category.

Category F: $R_2 \approx 1$, $\Delta \approx 1$

Two materials belonging to this category are $\text{Ag}_2\text{SO}_4 \cdot 4\text{NH}_3$, whose focusing pattern is shown in Fig. 1(b), and AgClO_3 . While they could be grouped with category D media, we have classified them separately since their focusing patterns bear a striking resemblance to those of cubic crystals such as CaF_2 .

Category G: $R_2 \approx 0$, $\Delta < 1$

The small value of $|R_2|$ correlates with $R_1 < 1$ and $R_4 < 1$ and for $\Delta=0$ there are no caustics at all. If the QT and PT sheets of S are nonintersecting, there remain no caustics even for finite, but small Δ . Vesuvian is an example of a tetragonal crystal devoid of caustics, which of course also implies the absence of conical points. This makes for an interesting contrast with cubic crystals which, except for the special case of perfect isotropy or

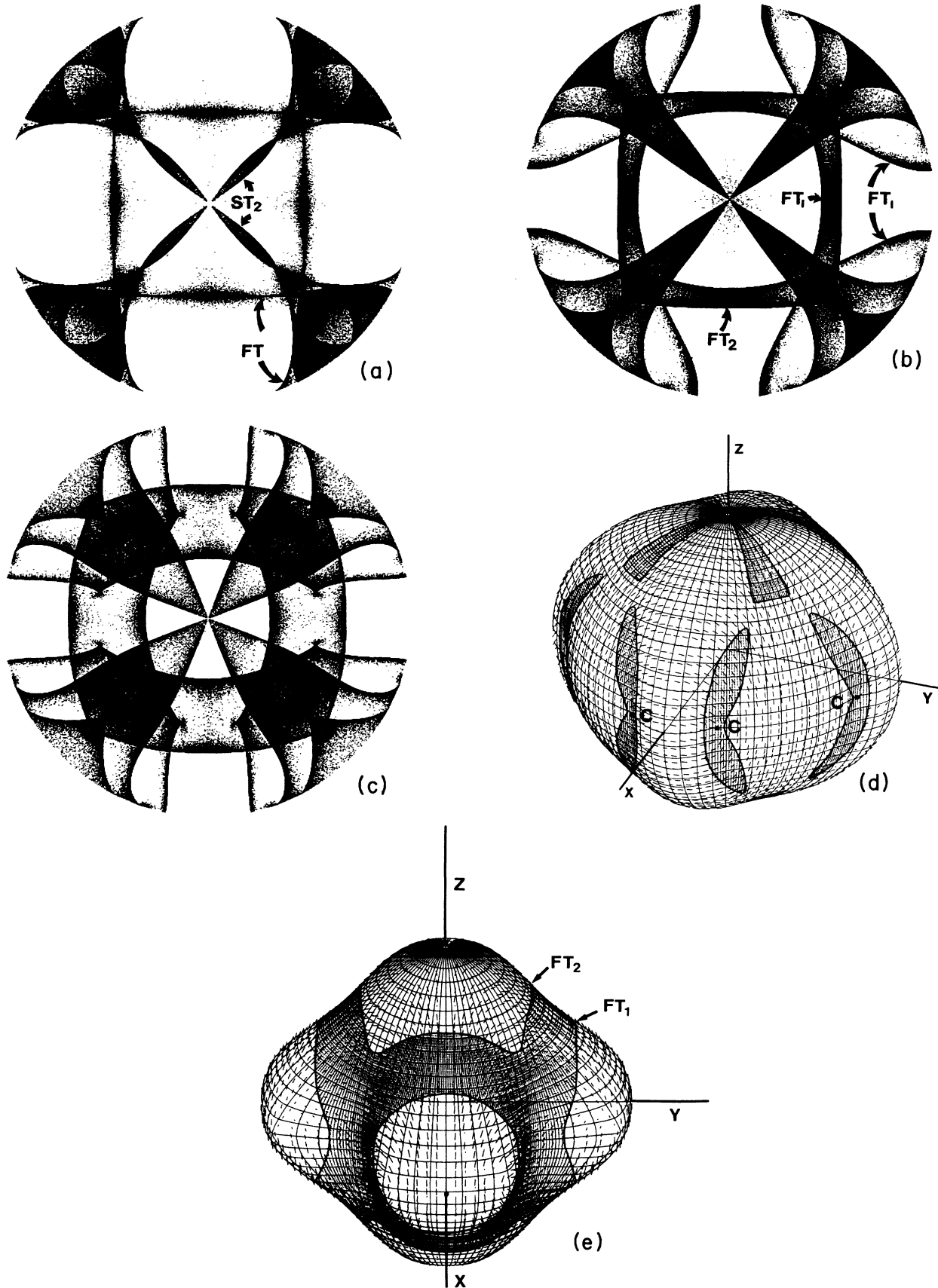


FIG. 8. ST and FT phonon intensity patterns for (a) K_2PtCl_4 , (b) CoF_2 , and (c) RbD_2AsO_4 . (d) ST sheet of the slowness surface of K_2PtCl_4 . (e) FT sheet of the slowness surface of CoF_2 . Shaded areas in (d) and (e) indicate where the surface is negatively curved.

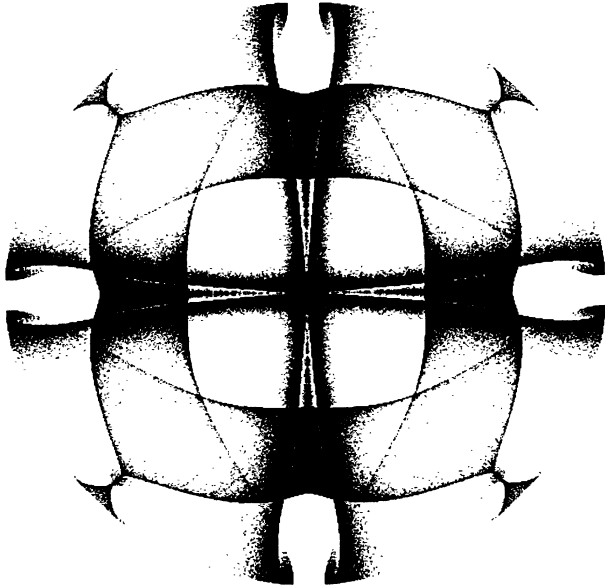


FIG. 9. ST and FT phonon intensity pattern for Hg_2Br_2 .

for $C_{12} + C_{44} = 0$, always have conical points and always display caustics.²

As Δ increases, sets of FT and ST precursors form in the region of the $\{100\}$ and $\{110\}$ planes. These evolve into caustic structures as Δ approaches ~ 0.5 . Figure 10(a) shows the focusing pattern of CsPbF_3 which is at this stage of development. Actually, $R_2 = -0.73$ for this material and the precursors to the waist-band caustics are also clearly in evidence.

If for $\Delta = 0$ the QT and PT sheets of S intersect, then avoided intersection caustics materialize as Δ deviates from zero. The focusing pattern of $\text{Ba}_2\text{Si}_2\text{TiO}_8$, shown in Fig. 10(b) displays this structure.

Category H: $R_2 \approx 0.5, \Delta \approx 4$

Figure 11 shows the focusing pattern of LiYF_4 . There is only one set of caustics, and these have developed as a result of the large value of Δ . There are no avoided intersection caustics or caustics derived from the polar anisotropy. Tin has a similar focusing pattern.

Category I: $R_2 \approx 0, \Delta \approx 4$

Here too, all the caustics have developed as a result of the large value of Δ . Figure 12(a) shows the focusing pattern and Fig. 12(b) shows a set of symmetry plane slowness curves for ZnP_2 . This is another example of a material for which the polarization field near the $[001]$ direction has rotary index $n = -1$, to which can be attributed the four-petal ST structure at the center of the focusing pattern. There are pairs of $n = +\frac{1}{2}$ conical points located in each quadrant of the (001) plane. Neighboring negatively curved regions of the ST sheet of S account for the structures that connect via precursors to the tips of the petals. The larger overlapping structures are due to negatively curved portions of the FT sheet in the neighbor-

hood of the $\langle 110 \rangle$ directions.

Crystals with similar focusing patterns are PbMoO_4 , SrMoO_4 , and zircon. In the last mentioned, the precursors have developed into caustics.

Category J: $R_2 \approx 0, \Delta \approx 10$

The large value of Δ is the determining factor in shaping the distended pattern of caustics. Figure 13 shows the focusing pattern of deuterated $\text{NH}_4\text{H}_2\text{PO}_4$ which falls into this category.

Category K: $C_{13} + C_{44} \approx 0, C_{12} + C_{66} \approx 0$

In the limit $C_{13} + C_{44} = C_{12} + C_{66} = 0$ the off-diagonal elements of the Christoffel matrix Γ_{rs} all vanish, the $X, Y,$

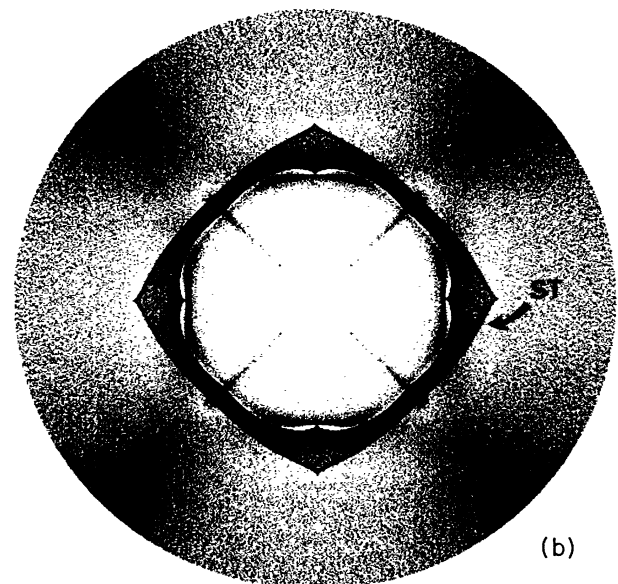
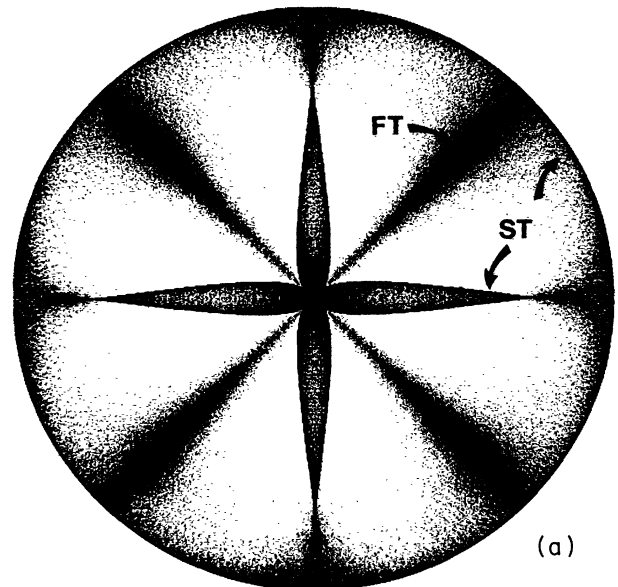


FIG. 10. ST and FT phonon intensity pattern for (a) CsPbF_3 and (b) $\text{Ba}_2\text{Si}_2\text{TiO}_8$.

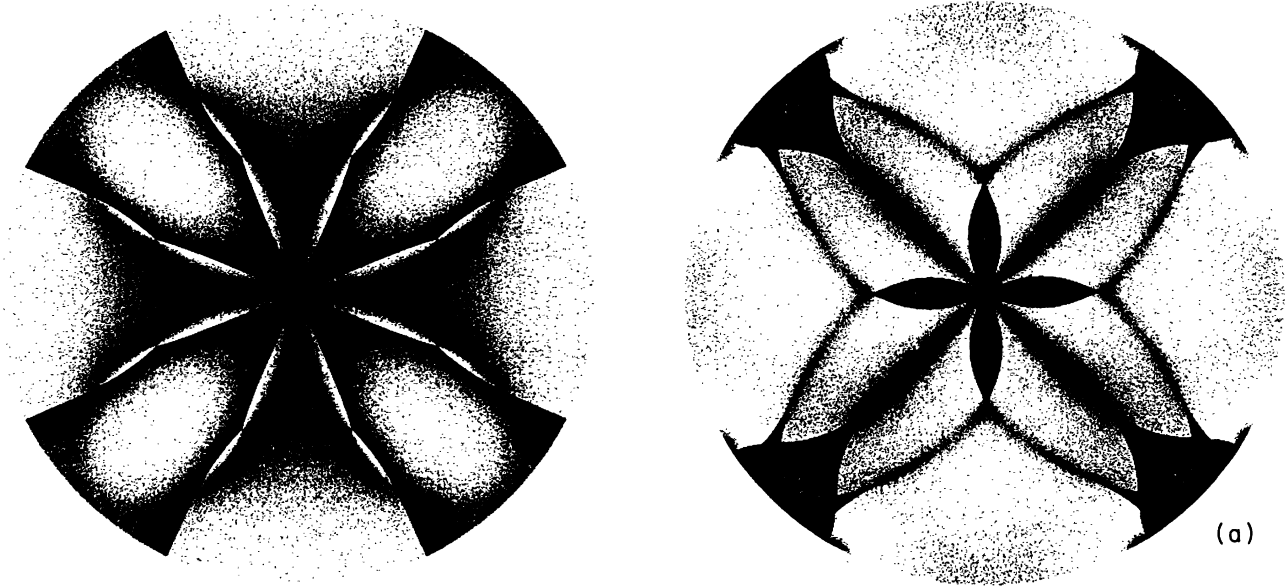


FIG. 11. ST and FT phonon intensity pattern for LiYF_4 .

and Z displacements are uncoupled and the equation of the slowness surface factorizes into that for three intersecting ellipsoids:

$$\begin{aligned} C_{11}S_x^2 + C_{66}S_y^2 + C_{44}S_z^2 &= \rho \quad (\text{all modes } X \text{ polarized}), \\ C_{66}S_x^2 + C_{11}S_y^2 + C_{44}S_z^2 &= \rho \quad (\text{all modes } Y \text{ polarized}), \\ C_{44}S_x^2 + C_{44}S_y^2 + C_{33}S_z^2 &= \rho \quad (\text{all modes } Z \text{ polarized}). \end{aligned} \quad (9)$$

Figure 14 shows a set of symmetry plane slowness curves for a hypothetical material satisfying these conditions and having $C_{44} > C_{66}$. The first and second ellipsoids intersect along ellipses in the $\{110\}$ planes, the first and third intersect along loops encircling the $[100]$ axis, and the second and third intersect along loops encircling the $[010]$ axis. For $C_{66} > C_{44}$ the second and third ellipsoids are reduced in size relative to the first, and they intersect the first along loops encircling the $[001]$ axis.

The three ellipsoids are entirely convex and so there are no caustics whatsoever. Immediately when $C_{13} + C_{44}$ and $C_{12} + C_{66}$ deviate from zero, the three sheets of S separate except at a finite set of point degeneracies, and avoided intersection caustics materialize. Figure 15(a) shows the focusing pattern for the medial and slow sheets of a hypothetical medium satisfying $C_{13} + C_{44} = C_{12} + C_{66} = 0$ (it would not be accurate to call them FT and ST). Were the fast mode phonon intensity (associated with the hatched segments of Fig. 14) to be included, the square-shaped regions of missing flux would be filled in and the intensity would everywhere be continuous. There are no caustics. Figure 15(b) shows the medial and slow sheet focusing pattern of CsH_2AsO_4 , which retains a strong resemblance to that of Fig. 15(a). The presence of the caustics, and the rounding of some of the squares of low

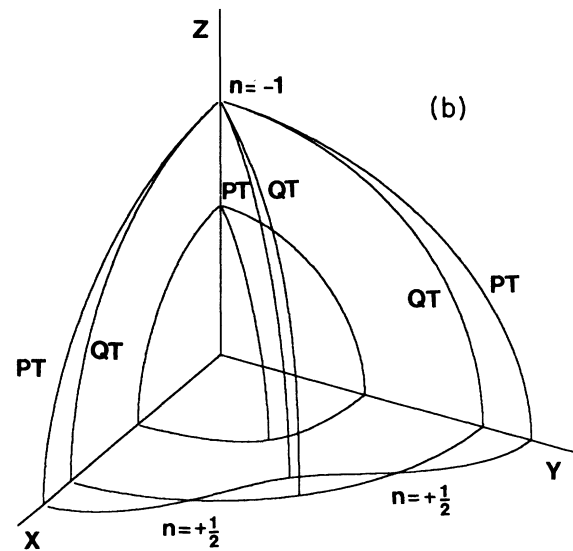


FIG. 12. (a) ST and FT phonon intensity pattern for ZnP_2 , (b) symmetry plane slowness curves for ZnP_2 .

phonon intensity is due to the deviation of $C_{13} + C_{44}$ and $C_{12} + C_{66}$ from zero.

V. DISCUSSION AND CONCLUSIONS

In the long-wavelength limit and the absence of piezoelectricity, the phonon-focusing patterns of tetragonal crystals are governed by five elastic constant ratios. Even within the bounds imposed by the thermodynamic constraints on the elastic constants, this permits considerable variety. In this paper we have not attempted to classify and describe in minute detail the multitude of focusing patterns that can occur. Our aim rather has

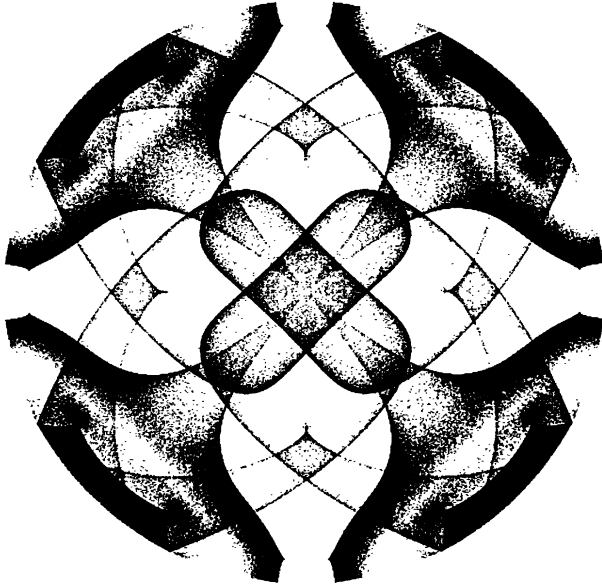
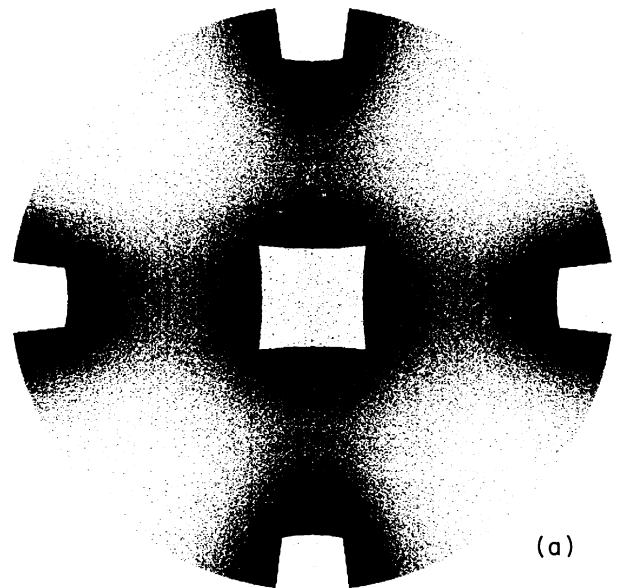


FIG. 13. ST and FT phonon intensity pattern for $\text{NH}_4\text{H}_2\text{PO}_4$ (44% deuterated).

been to present a reasonably compact and broad classification scheme that encompasses all tetragonal crystals on which data is readily available as well as neighboring regions of elastic constant space. The classification scheme we have put forward is not unique but it does at least bring some order to the assortment of focusing patterns there are, and shows that the problem is manageable. We have grouped together focusing patterns which have obvious overall similarities or are close-

ly related in some sense. With few exceptions however, the patterns in each category are not identical but all possess minor distinguishing features.

We have also shown that in broad outline even the most complex focusing patterns of tetragonal crystals can be traced to much simpler focusing patterns by the adjusting of one or two parameters. In most cases we have found a comparison with transverse isotropy to be illuminating. Here the values of the two parameters R_2 and Δ turn out to be a very good indicator of the focusing pattern. This is particularly so when $|R_2| > 1$ and $\Delta > 1$, which tends to stabilize the focusing pattern into



(a)

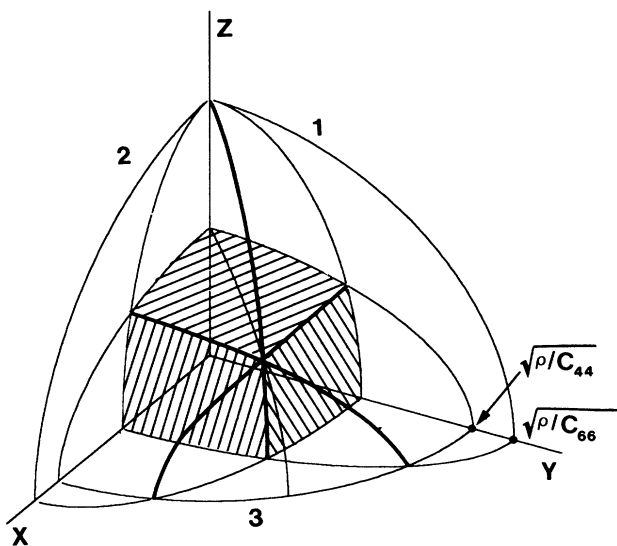
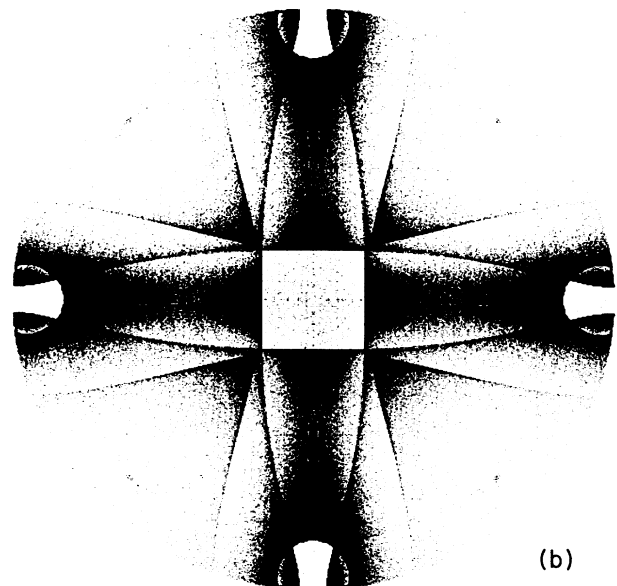


FIG. 14. Slowness curves for a hypothetical medium with $C_{11}=4$, $C_{33}=3$, $C_{66}=0.5$, $C_{12}=-0.5$, $C_{13}=-1$, all in units of C_{44} . The slowness surface consists of three ellipsoids which intersect along the heavy lines.



(b)

FIG. 15. Medial and slow sheets' phonon intensity pattern for (a) the same medium as in Fig. 14 and (b) CsH_2AsO_4 .

category B or D. Indeed nearly 50% of tabulated crystals fall into one or other of these two categories. For small $|R_2|$ and/or Δ there is more variability, and the influence of the individual elastic constant ratios is greater.

The focusing patterns of some crystals are better understood as approximating the condition where the slowest surface takes the form of three intersecting ellipsoids.

In a very small number of cases, notably urea (category

B) and $\text{LiY}_{0.5}\text{Tb}_{0.5}\text{F}_4$ (category H), crystals which arguably could be put into categories of their own we have preferred to assign to larger categories.

The calculations we have done for a variety of hypothetical crystals suggest that the great majority of "ordinary" tetragonal crystals will fit into the classification scheme we have proposed here. Should, however, "unusual" crystals with properties such as $C_{11}, C_{33} < C_{44}, C_{66}$ be found, it might be necessary to expand the classification scheme to accommodate them.

- ¹For recent reviews on phonon focusing and phonon imaging see, G. A. Northrop and J. P. Wolfe, in *Nonequilibrium Phonon Dynamics*, edited by W. E. Bron (Plenum, New York, 1985), p. 165; H. J. Maris, in *Nonequilibrium Phonons in Non-Metallic Crystals*, edited by W. Eisenmenger and A. A. Kaplyanskii (North-Holland, Amsterdam, 1986), p. 51.
- ²A. G. Every, *Phys. Rev. B* **24**, 3456 (1981); A. G. Every and A. J. Stoddart, *ibid.* **32**, 1319 (1985).
- ³D. C. Hurley and J. P. Wolfe, *Phys. Rev. B* **32**, 2568 (1985).
- ⁴L. A. Chernosatonskii and V. V. Novikov, *Phys. Lett. A* **117**, 349 (1986); V. V. Novikov and L. A. Chernosatonskii, *Fiz. Tverd. Tela (Leningrad)* **28**, 2238 (1986) [*Sov. Phys.—Solid State* **28**, 1255 (1986)].
- ⁵A. K. McCurdy, *Phys. Rev. B* **9**, 466 (1974).
- ⁶A. G. Every, *Phys. Rev. B* **34**, 2852 (1986).
- ⁷A. G. Every and A. K. McCurdy, *Phys. Rev. B* **36**, 1432 (1987).
- ⁸A. G. Every, *Phys. Rev. B* **36**, 1448 (1987).
- ⁹See, for example, G. A. Northrop, *Phys. Rev. B* **26**, 903 (1982); G. A. Northrop, S. E. Hebboul, and J. P. Wolfe, *Phys. Rev. Lett.* **55**, 95 (1985); S. E. Hebboul and J. P. Wolfe, *Phys. Rev. B* **34**, 3948 (1986).
- ¹⁰C. G. Winternheimer and A. K. McCurdy, *Phys. Rev. B* **18**, 6576 (1978).
- ¹¹M. J. P. Musgrave, *Proc. Cambridge Philos. Soc.* **53**, 897 (1957); *J. Elasticity* **9**, 105 (1979).
- ¹²R. F. S. Hearmon, in *Numerical Data and Functional Rela-*

tionships in Science and Technology, New Series, Vol. 11, Group III of *Landolt-Börnstein*, edited by K. H. Hellwege (Springer, Berlin, 1979), pp. 1–244; *Numerical Data and Functional Relationships in Science and Technology*, Vol. 18, Group III of *Landolt-Börnstein*, edited by K. H. Hellwege (Springer, Berlin, 1984), pp. 1–154.

- ¹³G. A. Northrop and J. P. Wolfe, *Phys. Rev. B* **22**, 6196 (1980).
- ¹⁴H. J. Maris, *J. Acoust. Soc. Am.* **50**, 812 (1971).
- ¹⁵See, for example, R. Eichele, R. P. Huebener, and H. Seifert, *Z. Phys. B* **48**, 89 (1982); H. Kinder, in *Nonequilibrium Phonon Dynamics*, edited by W. E. Bron (Plenum, New York, 1985), p. 129; A. G. Every, G. L. Koos, and J. P. Wolfe, *Phys. Rev. B* **29**, 2190 (1984).
- ¹⁶D. C. Hurley, J. P. Wolfe, and K. A. McCarthy, *Phys. Rev. B* **33**, 4189 (1986).
- ¹⁷F. I. Fedorov, *Theory of Elastic Waves in Crystals* (Plenum, New York, 1968).
- ¹⁸M. J. P. Musgrave, *Crystal Acoustics* (Holden-Day, San Francisco, 1970).
- ¹⁹B. A. Auld, *Acoustic Fields and Waves in Solids* (Wiley, New York, 1973).
- ²⁰A. G. Every, *J. Phys. C* **20**, 2973 (1987).
- ²¹M. J. P. Musgrave, *Acta. Cryst.* **10**, 316 (1957); M. J. P. Musgrave, *Proc. R. Soc. London Ser. A* **401**, 131 (1985).
- ²²V. I. Al'shits and A. L. Shulvalov, *Kristallografiya* **29**, 629 (1984) [*Sov. Phys.—Crystallogr.* **29**, 373 (1984)].

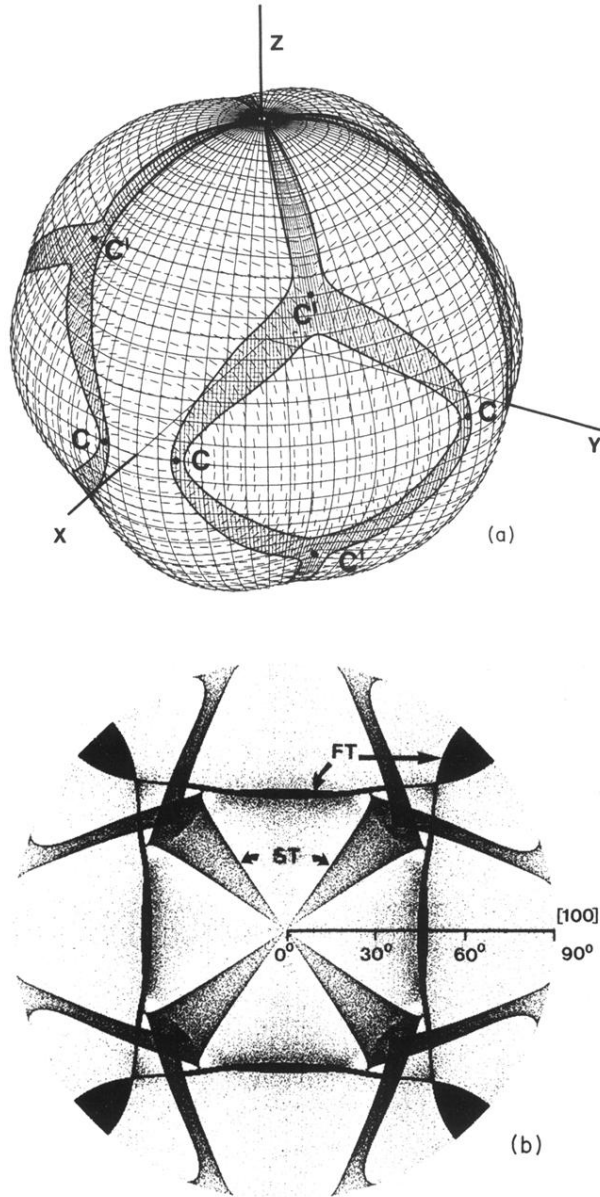


FIG. 1. (a) ST sheet of the acoustic slowness surface of $\text{Ag}_2\text{SO}_4 \cdot 4\text{NH}_3$. The shaded areas represent regions of negative Gaussian curvature, the remainder of the surface being of positive curvature. The polarization field displays singularities at two sets of conical points labeled C and C' . The surface is negatively curved in the region of these conical points. (b) Polar plot of the ST and FT phonon intensity for $\text{Ag}_2\text{SO}_4 \cdot 4\text{NH}_3$. Darkness of the greyscale represents the phonon intensity. Caustics are labeled according to branch. The ST caustics are mapped from the lines of zero Gaussian curvature separating the negatively and positively curved portions of the surface in (a).

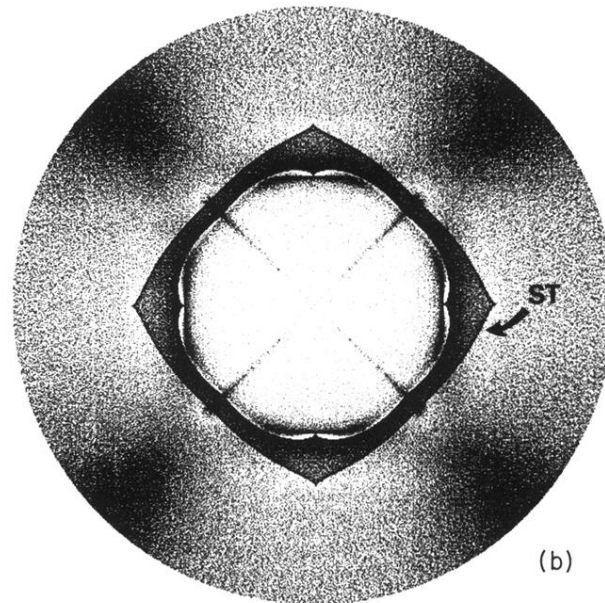
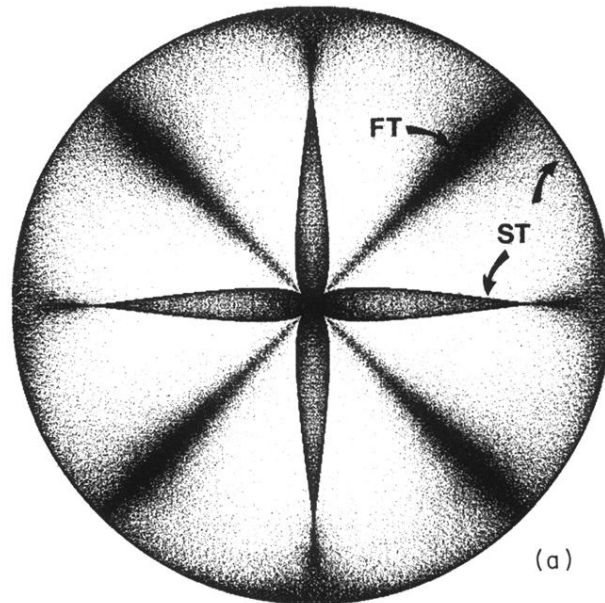


FIG. 10. ST and FT phonon intensity pattern for (a) CsPbF₃ and (b) Ba₂Si₂TiO₈.

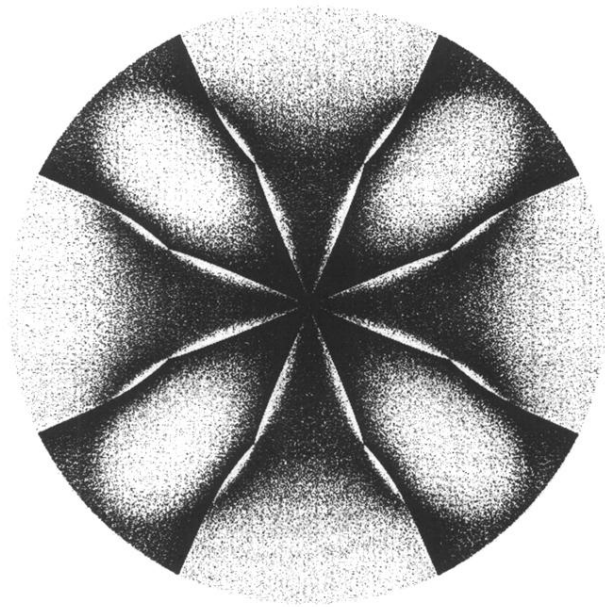


FIG. 11. ST and FT phonon intensity pattern for LiYF₄.

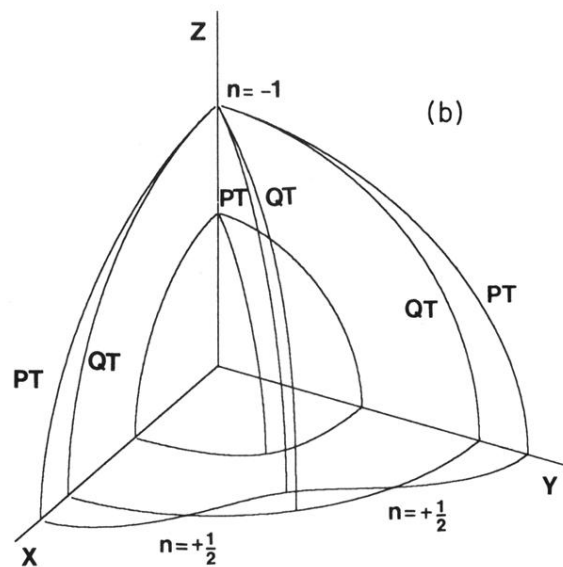
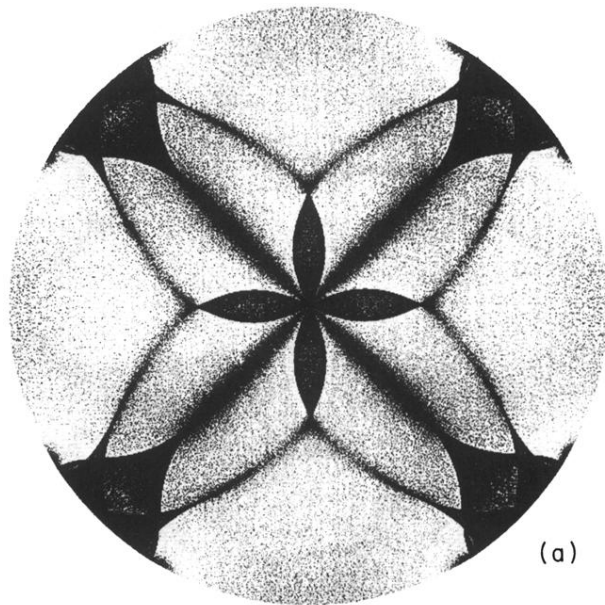


FIG. 12. (a) ST and FT phonon intensity pattern for ZnP_2 ,
 (b) symmetry plane slowness curves for ZnP_2 .

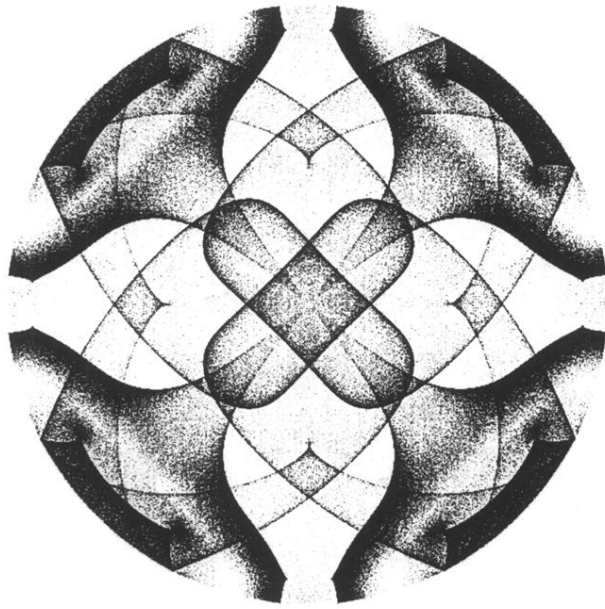


FIG. 13. ST and FT phonon intensity pattern for $\text{NH}_4\text{H}_2\text{PO}_4$ (44% deuterated).

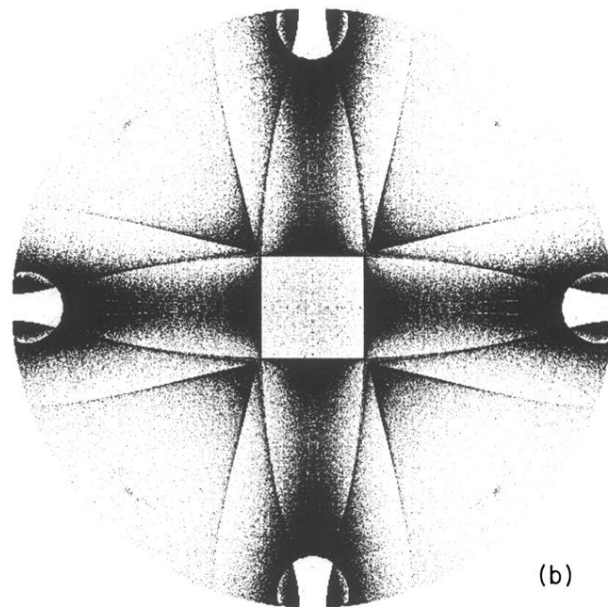
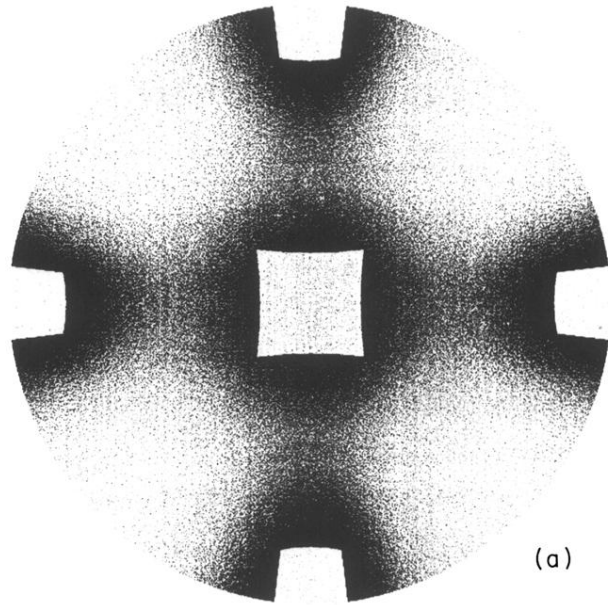


FIG. 15. Medial and slow sheets' phonon intensity pattern for (a) the same medium as in Fig. 14 and (b) CsH_2AsO_4 .

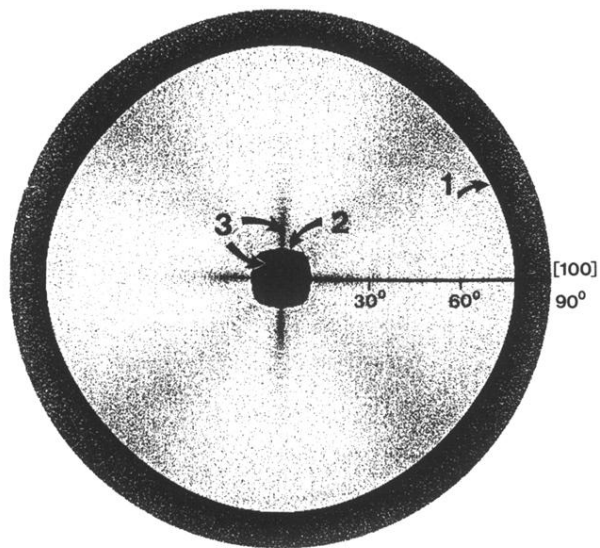
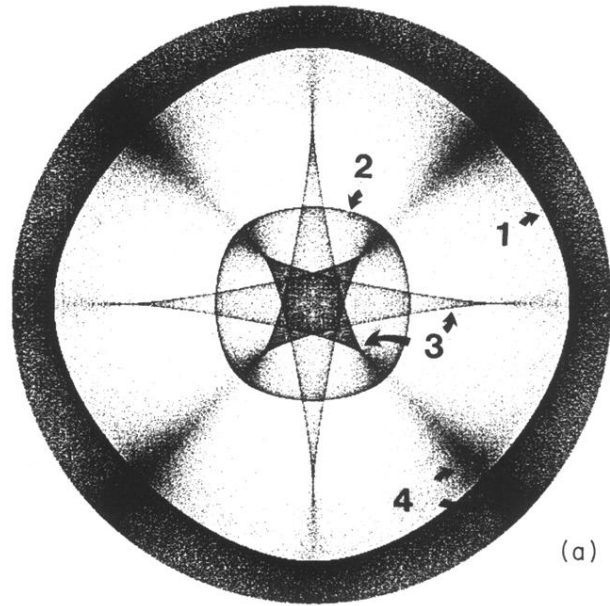
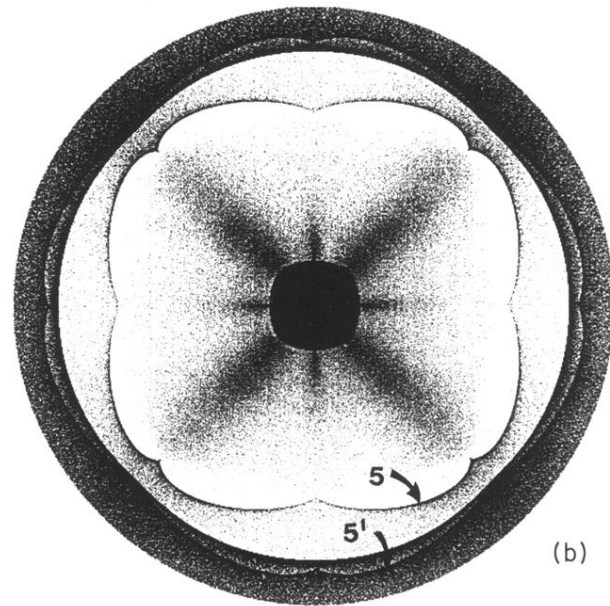


FIG. 4. Polar plot of the ST and FT phonon intensity for terbium molybdate ($\Delta=0.16$).



(a)



(b)

FIG. 5. ST and FT phonon intensity pattern for (a) a hypothetical medium with $C_{11}=4$, $C_{33}=2$, $C_{66}=1.5$, $C_{12}=0.4$, and $C_{13}=2$ and (b) a hypothetical medium with $C_{11}=4$, $C_{33}=4$, $C_{66}=0.7$, $C_{12}=2.5$, and $C_{13}=3$. All elastic constants are in units of C_{44} .

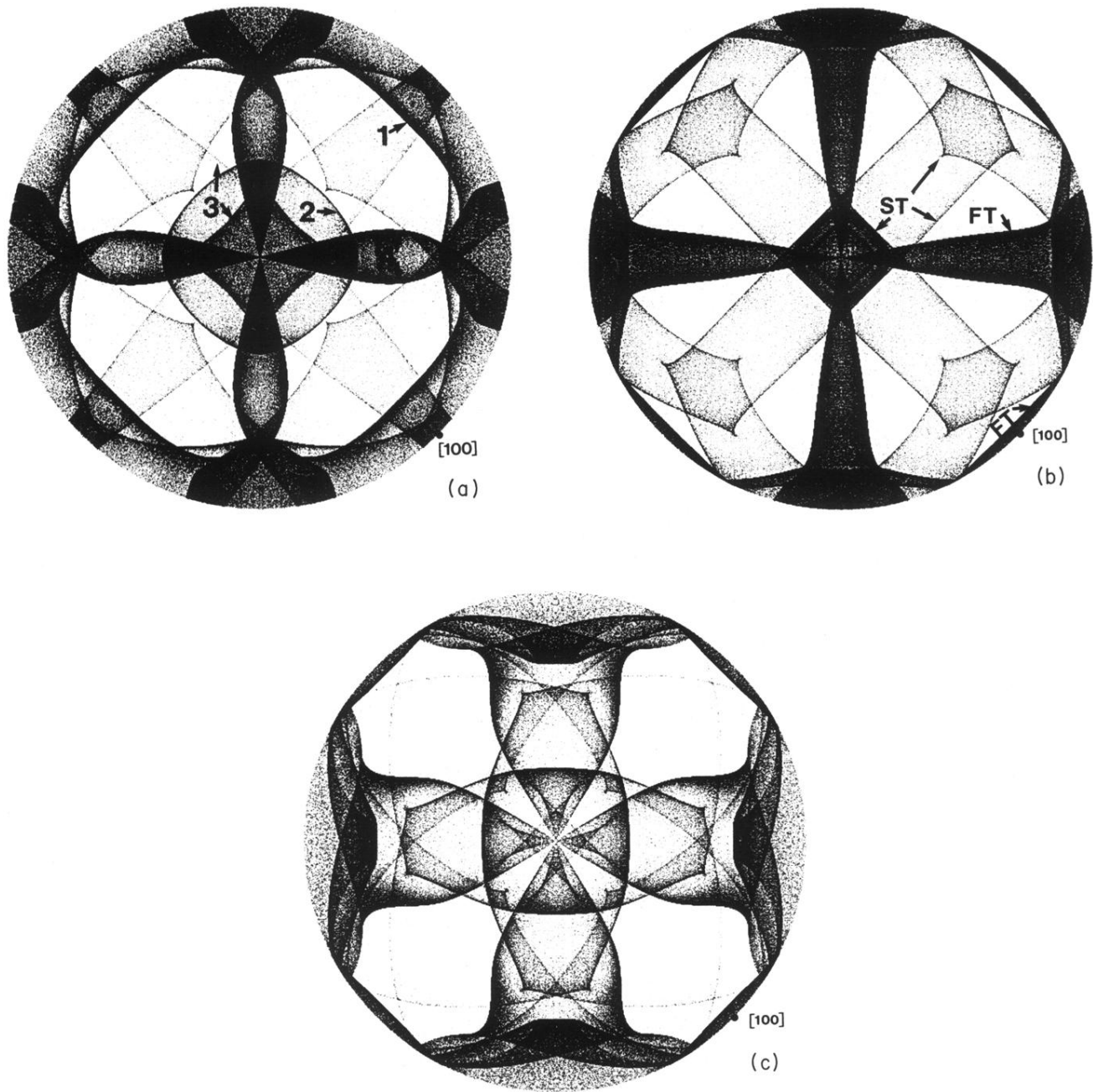


FIG. 6. ST and FT phonon intensity pattern for (a) InBi, (b) AgGaS₂, and (c) In-3.4 at. %-Cd alloy.

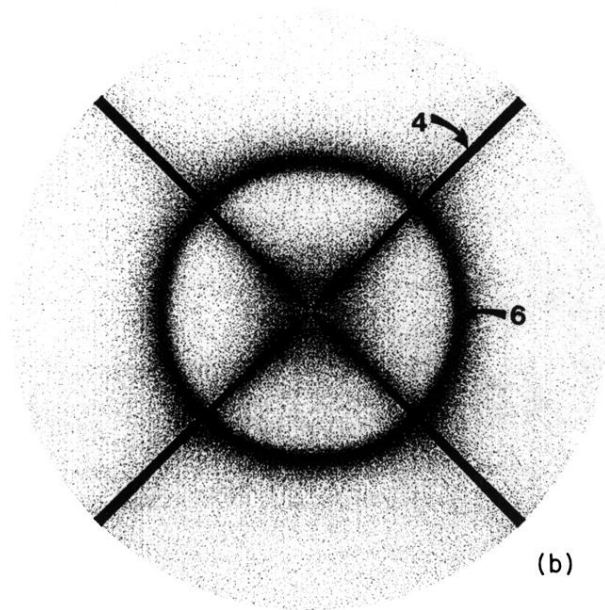
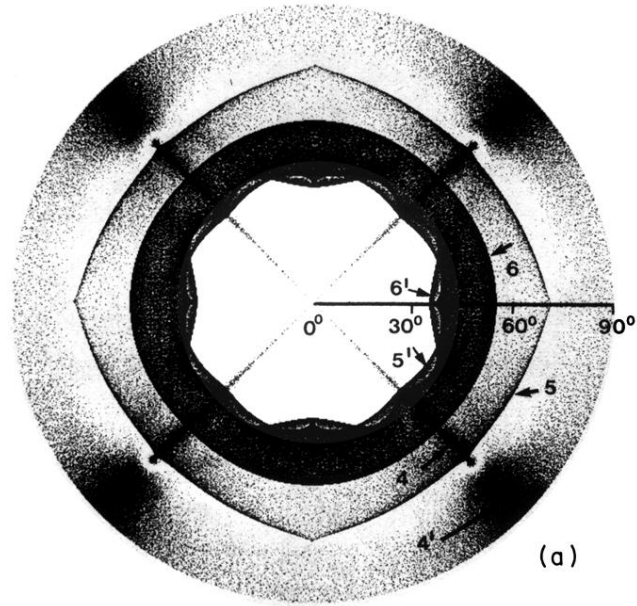


FIG. 7. ST and FT phonon intensity pattern for (a) Al_2Cu , (b) Zr_2Ni ($R_2 = 1.07$, $\Delta = 0.80$).

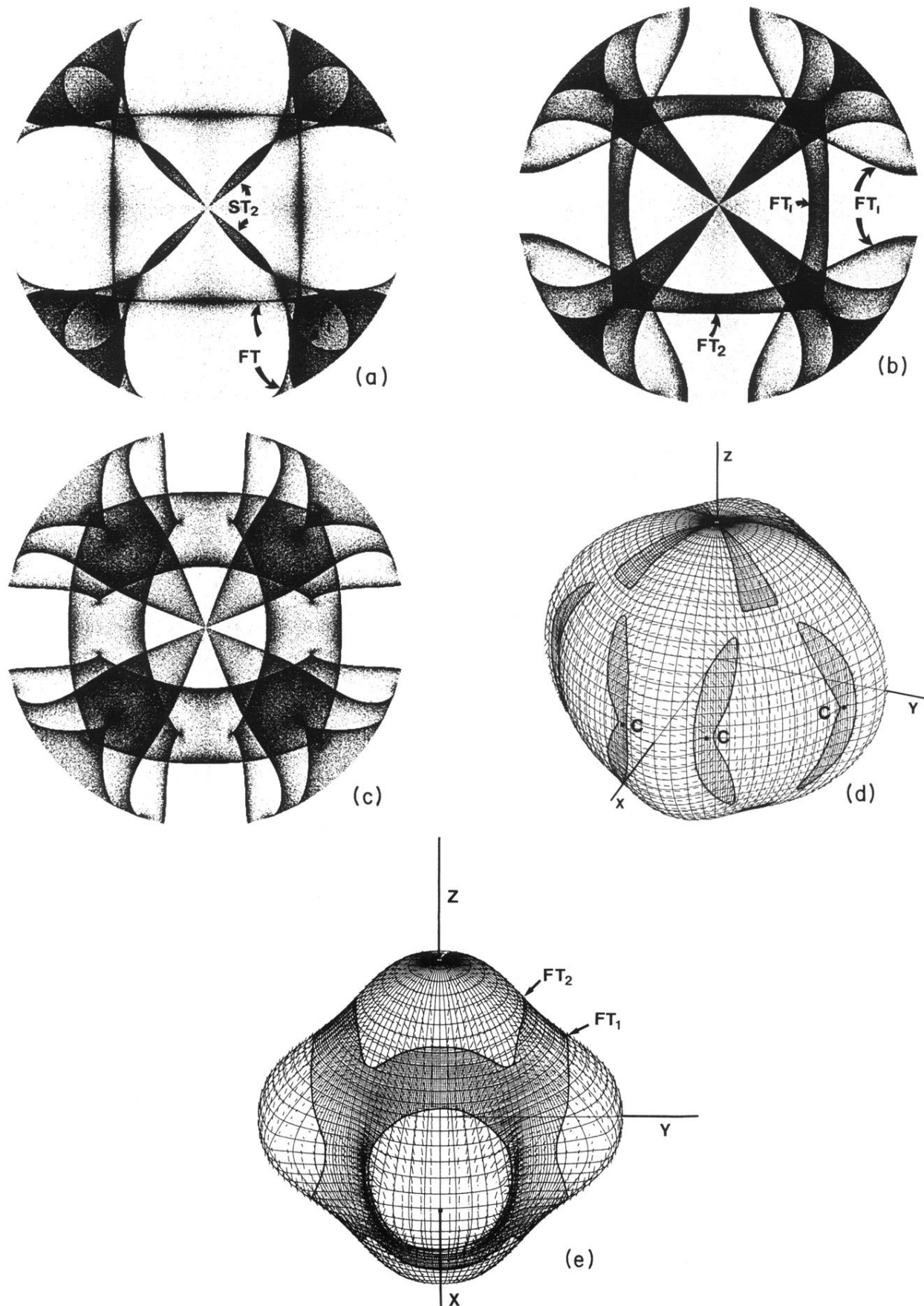


FIG. 8. ST and FT phonon intensity patterns for (a) K_2PtCl_4 , (b) CoF_2 , and (c) RbD_2AsO_4 . (d) ST sheet of the slowness surface of K_2PtCl_4 . (e) FT sheet of the slowness surface of CoF_2 . Shaded areas in (d) and (e) indicate where the surface is negatively curved.

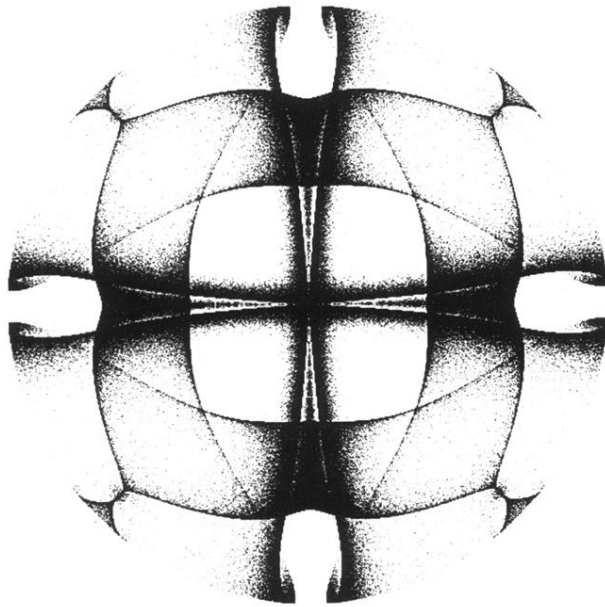


FIG. 9. ST and FT phonon intensity pattern for Hg₂Br₂.